



Trans. Nonferrous Met. Soc. China 25(2015) 3736-3746

Transactions of Nonferrous Metals Society of China

www.tnmsc.cn



# Electrochemical properties of nanocrystalline and amorphous Mg-Y-Ni alloys applied to Ni-MH battery

Yang-huan ZHANG<sup>1,2</sup>, Zhong-gang HAN<sup>1,2</sup>, Ze-ming YUAN<sup>2</sup>, Tai YANG<sup>2</sup>, Yan QI<sup>2</sup>, Dong-liang ZHAO<sup>2</sup>

- 1. Key Laboratory of Integrated Exploitation of Baiyun Obo Multi-Metal Resources, Inner Mongolia University of Science and Technology, Baotou 014010, China;
- 2. Department of Functional Material Research, Central Iron and Steel Research Institute, Beijing 100081, China

Received 15 December 2014; accepted 17 March 2015

**Abstract:** The as-cast  $Mg_2Ni$ -type  $Mg_{20-x}Y_xNi_{10}$  (x=0, 1, 2, 3 and 4) electrode alloys were prepared by vacuum induction melting. Subsequently, the as-cast alloys were mechanically milled in a planetary-type ball mill. The analyses of scanning electron microscopy (SEM), X-ray diffraction (XRD) and transmission electron microscopy (TEM) reveal that nanocrystalline and amorphous structure can be obtained by mechanical milling, and the amount of amorphous phase increases with milling time prolonging. The electrochemical measurements show that the discharge capacity of  $Y_0$  alloy increases with milling time prolonging, while that of the Y-substituted alloys has a maximum value in the same condition. The cycle stabilities of the alloys decrease with milling time prolonging. The effect of milling time on the electrochemical kinetics of the alloys is related to Y content. When x=0, the high rate discharge ability, diffusion coefficient of hydrogen atom, limiting current density and charge transfer rate all increase with milling time prolonging, but the results are exactly opposite when x=3.

Key words: hydrogen storage; Mg<sub>2</sub>Ni-type alloy; mechanical milling; element substitution; electrochemical performance

# 1 Introduction

Mg<sub>2</sub>Ni-type hydrogen storage alloys and their hydrides have been deemed to be one of the most promising hydrogen storage materials applied in hydrogen fuel cell vehicle or negative electrodes in Ni-MH batteries [1,2] because of their major advantages, such as the high gaseous hydrogen absorption capacity (3.6%) for Mg<sub>2</sub>NiH<sub>4</sub> and the large gravimetric capacity (about 1000 mA·h/g) [3]. However, the practical applications of Mg<sub>2</sub>Ni-type alloy for Ni-MH batteries are full of challenges because of some innate shortcomings, such as sluggish hydriding/dehydriding kinetics, low electrochemical discharge capacity relatively to the theoretical value at room temperature and poor cycle stability in alkaline solution. The strategy for improving the hydrogen sorption properties of Mg-based alloys can be divided into two categories: firstly, alloying with other elements such as transition metals, rare-earth (RE) metals and transition metal oxides; secondly, applying different preparation technologies to modify the structure of the alloy. JURCZYK et al [4] reported that the addition or partial substitution of elements has been proved very effective electrochemical properties of Mg2Ni-type alloy. The obtained by WOO and LEE [5] and TAKAHASHI et al [6] revealed that the partial substitution of elements (Cu, Fe, V, Cr, Co) for Ni in Mg<sub>2</sub>Ni compound decreases the stability of the hydride and makes the desorption reaction easy. Also, rare earth element additives were found to improve the electrode characteristics, particularly the cycle life, which can be attributed to the increased corrosion resistance [7]. Furthermore, it was documented that the hydriding and dehydriding kinetics of the Mg and Mg-based alloys are very sensitive to their structures [8]. WANG et al [9] reported that nanocrystalline and amorphous Mg-based hydrogen storage alloys showed high hydrogen absorption capacity at low temperatures and ambient pressure, and better kinetics of hydriding and dehydriding compared with their bulk counterparts. Mechanical milling [10] and melt-spinning [11,12] are proved to be extremely appropriate techniques for

producing amorphous and nanocrystalline Mg-based alloys with different compositions. In our previous studies, Mg-based alloys with nanocrystalline and amorphous structure produced by melt-spinning exhibit excellent hydriding characteristics [13,14]. microstructure created by melt spinning displays good stability during the hydrogen absorbing and desorbing cycles [15]. Compared with melt spinning, some inherent shortcomings of ball milling technology seem to be unavoidable: the milled materials are easily polluted by steel balls and air, even though in very good protection conditions. However, ball milling can improve the thermodynamics of the hydriding and dehydriding reactions by introducing capillarity effects because the particle size can be reduced to a small enough size [16].

In the present work, the  $Mg_2Ni$ -type  $Mg_{20-x}Y_xNi_{10}$  (x=0-4) alloys were prepared by mechanical ball milling, and the effects of milling time on the structures and electrochemical performances of the alloys were investigated.

## 2 Experimental

The experimental alloys with the chemical composition of the  $Mg_{20-x}Y_xNi_{10}$  (x=0, 1, 2, 3 and 4) were prepared using a vacuum induction furnace under a helium atmosphere at a pressure of 0.04 MPa to prevent Mg from volatilizing. The molten alloy was poured into a copper mould cooled by water, thus a cast ingot was obtained. A part of the as-cast alloys was mechanically crushed into powder with a particle size of about 50 µm. Then, the prepared powder was mechanically milled in a planetary-type mill in the argon protection environment to prevent the powders from being oxidized during ball milling. The samples were also handled in a glove box under Ar atmosphere. Cr-Ni stainless steel balls and the powders with a mass ratio of 35:1 were put into Cr-Ni stainless steel vials together. The milling speed was 135 r/min and the duration time was 10 and 70 h. For convenience of description, the alloys were denoted with Y content as  $Y_0$ ,  $Y_1$ ,  $Y_2$ ,  $Y_3$  and  $Y_4$ .

A Philips SEM (QUANTA 400) linked with an energy dispersive spectrometer (EDS) was used for examining morphologies and analyzing chemical composition of the as-cast alloys. The phase structures of the as-cast and milled alloys were determined by means of XRD (D/max/2400). The diffraction, with the experimental parameters of 160 mA, 40 kV and 10 (°)/min respectively, was performed with Cu K $_{\alpha}$  radiation filtered by graphite. The powder samples of the as-milled alloys were examined using high resolution TEM (JEM-2100F, operated at 200 kV) and their crystalline states were determined by electron diffraction (ED).

A mixture of the alloy powder and carbonyl nickel powder in a mass ratio of 1:4 was cold-pressed under a pressure of 35 MPa into round electrode pellets with a diameter of 15 mm whose total mass was 1 g. The electrochemical performances were measured at 303 K using a tri-electrode open cell consisting of a working electrode (the metal hydride electrode), a sintered Ni(OH)<sub>2</sub>/NiOOH counter electrode as well as a Hg/HgO reference electrode, which were immersed in 6 mol/L KOH electrolyte. The voltage between the negative electrode and the reference one was defined as the discharge voltage. In every cycle, the alloy electrode was first charged at a constant current density, and after resting for 15 min it was discharged at the same current density to cut-off voltage of –500 mV.

To determine the electrochemical kinetics of the alloy electrodes, the electrochemical impedance spectra (EIS) and the Tafel polarization curves of the alloys were measured at 303 K using an electrochemical workstation (PARSTAT 2273). Prior to measurement, several electrochemical charging and discharging cycles were carried out to activate the materials. The fresh electrodes were fully charged and then rested for 2 h up to the stabilization of the open circuit potential. The EIS of the alloy electrodes was measured at 50% depth of discharge (DOD), frequency range from 10 kHz to 5 mHz, amplitude of signal potentiostatic or galvanostatic measurements being 5 mV and the number of points per decade of frequencies being 60. The Tafel polarization curves were measured in the potential range of -1.2 to +1.0 V (vs Hg/HgO) with a scan rate of 5 mV/s. For the potentiostatic discharge, the test electrodes in the fully charged state were discharged at 500 mV potential steps for 5000 s on electrochemical workstation (PARSTAT 2273), using electrochemistry corrosion software (CorrWare).

#### 3 Results and discussion

#### 3.1 Microstructure characteristics

Figure 1 shows the SEM images and EDS patterns of the as-cast  $Mg_{20-x}Y_xNi_{10}$  (x=0-4) alloys, from which it is found that all the as-cast alloys exhibit coarse structures and the substitution of Y for Mg brings on great change in the morphologies of the alloys. The as-cast  $Y_0$  alloy exhibits a typical dendritic structure, but the Y substitution for Mg (x=1) brings on the formation of the secondary phases  $Mg_3Y$  and  $YMgNi_4$  without altering the major phase  $Mg_2Ni$ . With Y content increasing to x=3, the major phase changes into  $YMgNi_4$ , with a small amount of secondary phases  $Mg_2Ni$  and  $Mg_3Y$ .

The XRD patterns of the as-cast and milled  $Y_0$  and  $Y_3$  alloys are depicted in Fig. 2. Evidently, the

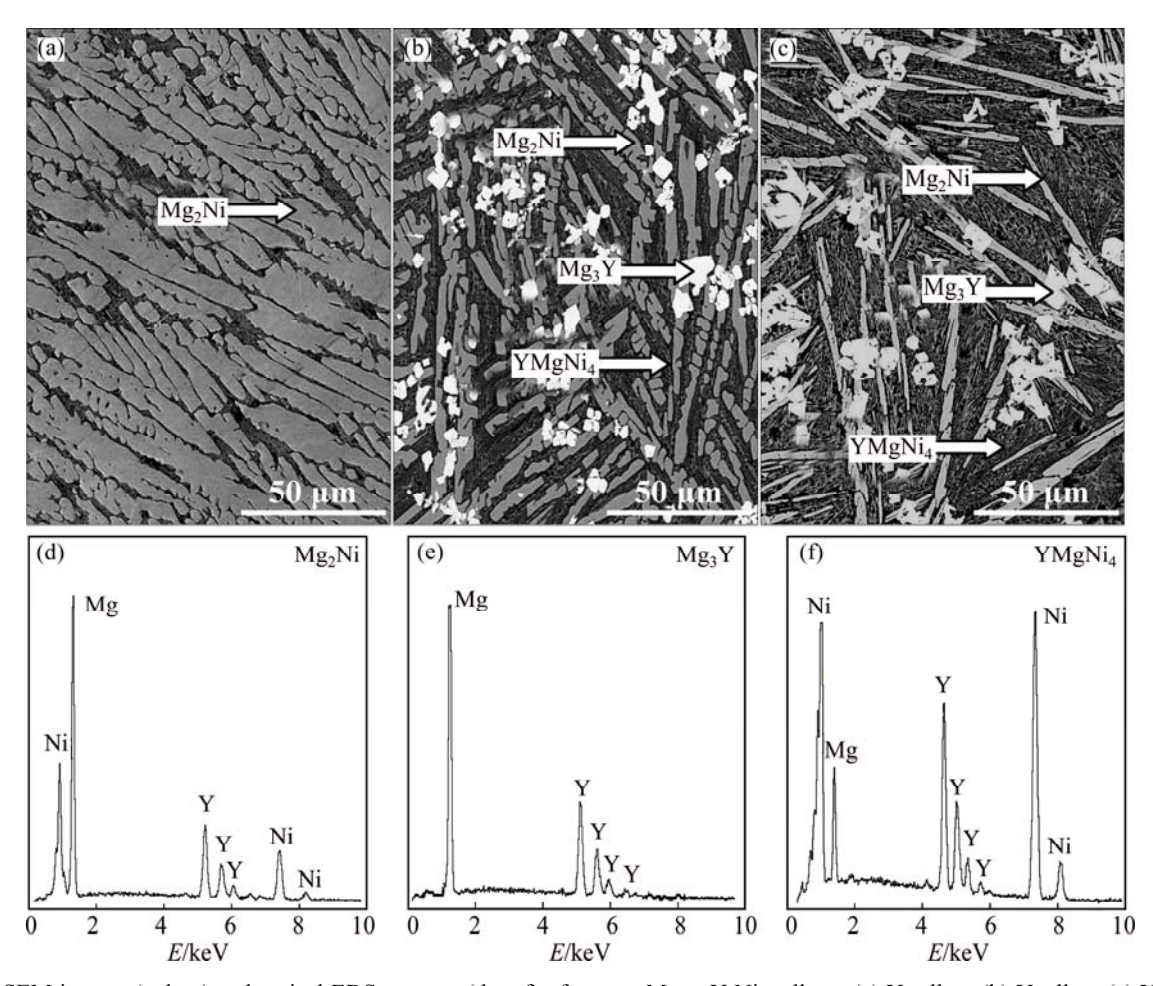


Fig. 1 SEM images (a, b, c) and typical EDS patterns (d, e, f) of as-cast  $Mg_{20-x}Y_xNi_{10}$  alloys: (a)  $Y_0$  alloy; (b)  $Y_1$  alloy; (c)  $Y_3$  alloy; (d)  $Mg_2Ni$  phase; (e)  $Mg_3Y$  phase; (f)  $YMgNi_4$  phase

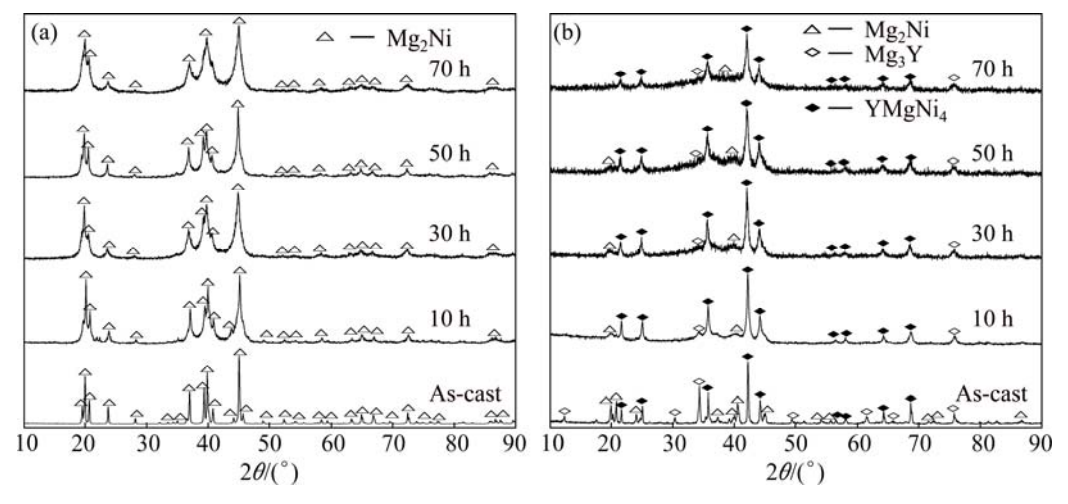
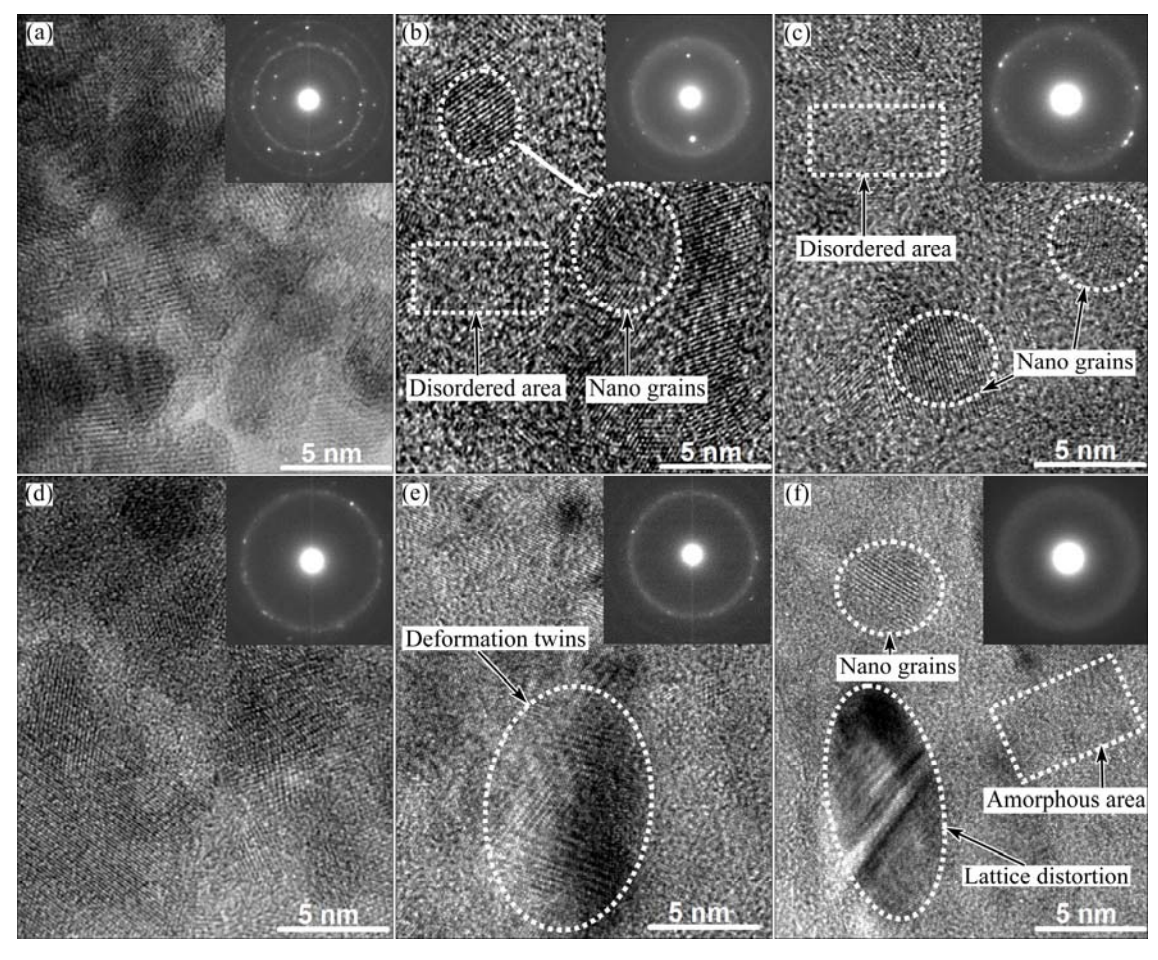


Fig. 2 XRD patterns of as-cast and milled  $Mg_{20-x}Y_xNi_{10}$  alloys: (a)  $Y_0$  alloy; (b)  $Y_3$  alloy

mechanical milling makes diffraction peaks of the alloys merge and dramatically broaden, which can be ascribed to the changes of crystal grain size and a heterogeneous strain. Meanwhile, we also find that the substitution of Y for Mg gives rise to an obvious change in the phase composition. Mechanical milling leads to the diffraction peaks of  $Mg_2Ni$  and  $Mg_3Y$  phases weakened or

disappeared. This may be that the Mg<sub>2</sub>Ni and Mg<sub>3</sub>Y phase are more easily transformed into amorphous structure in the process of ball milling.

The morphological characteristics of the as-milled  $Y_0$  and  $Y_3$  alloys are examined by TEM, just as shown in Fig. 3. It is noted that there is a clear change in the morphologies of the alloys with milling time prolonging.



**Fig. 3** TEM images and ED patterns of as-milled  $Mg_{20-x}Y_xNi_{10}$  (x=0-4) alloys: (a-c)  $Y_0$  alloys milled for 10, 30 and 50 h, respectively; (d-f)  $Y_3$  alloys milled for 10, 30 and 50 h, respectively

More specifically, a nearly entire nanocrystalline structure can be observed in the Y<sub>0</sub> and Y<sub>3</sub> alloys milled for 10 h, which is evidenced by Debye-Scherrer rings. When milling time increases to 30 h, Y<sub>0</sub> alloy still keeps a nanocrystalline structure, but some disordered structure areas can clearly be seen. Differing from the Y<sub>0</sub> alloy, the Y<sub>3</sub> alloy exhibits a nanocrystalline and amorphous structure, and crystal defects, e.g., deformation twins, can be observed. Further increasing milling time to 50 h, the structure of the Y<sub>0</sub> alloy is obviously refined and the disordered structure area significantly increases compared with Fig. 3(b). This is due to the fact that in the process of ball milling, powdered materials can be ground into very small particles. Frequent and intense action of impact, squeezing and fractionizing results in the creation of a large number of crystal defects. Meanwhile, we find that the Y<sub>3</sub> alloy shows a nanocrystalline and amorphous structure and the amount of the amorphous phase considerably grows compared with Fig. 3(e). In addition, the severe deformation and distortion of the crystal lattice caused by mechanical milling can be seen from Fig. 3(f). Particularly, after comparing Figs. 3(c) with (e), we can conclude that Y

substitution for Mg facilitates the glass forming of the  $Mg_2Ni$  alloy.

## 3.2 Electrochemical performance

## 3.2.1 Discharge potential and discharge capacity

Figure 4 shows the discharge potentials of the as-cast and milled  $Mg_{20-x}Y_xNi_{10}$  (x=0-4) alloy electrodes as a function of discharge capacity with a current density of 40 mA/g at the first charging/discharging cycle due to the fact that all the alloys can be easily activated to reach the maximum capacity at the first cycle. It is evident that for all the alloys the potentials visibly drop with discharge capacity increasing, meaning that the output power of Ni-MH battery is unstable. Hence, maintaining discharge potential at a relatively stable value is very important for the application of Ni-MH battery. Usually, the discharge potential characteristic is characterized by the potential plateau of the discharge curve of the alloy. The longer and more horizontal the discharge potential plateau is, the better the discharge potential characteristics of the alloy will be. It can be seen from Fig. 4 that milling time exerts an obvious effect on the discharge potential characteristic of the alloys. Here, we

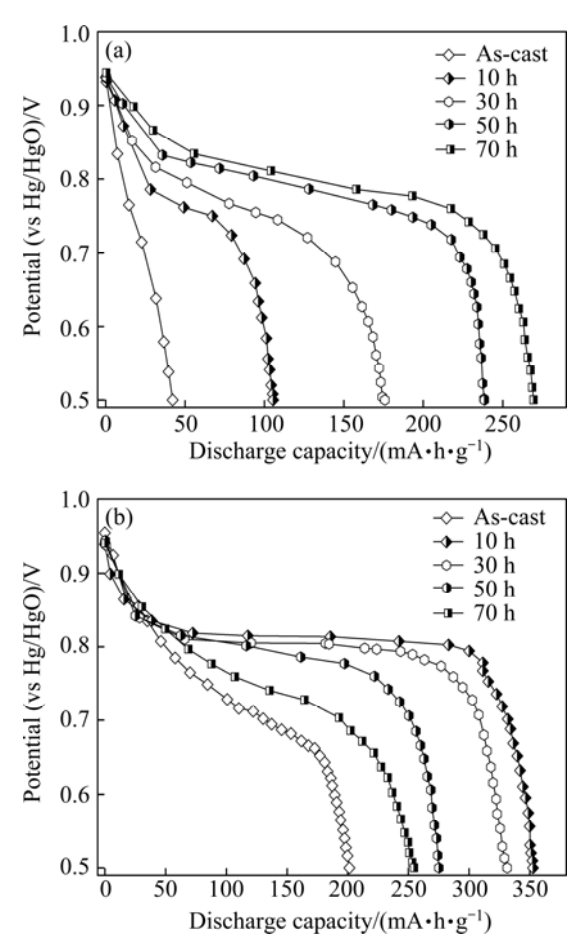


**Fig. 4** Discharge potential curves of as-cast and milled  $Y_0$  (a) and  $Y_3$  (b) alloys

define the milling time corresponding to the highest potential and the longest potential plateau as the optimal milling time. Obviously, for the  $Y_0$  alloy, the optimal milling time is 70 h, while for the  $Y_3$  alloy, it is 10 h. LAI and YU [17] considered that the discharge potential of an alloy electrode is basically dependent on its resistance, which is mainly dominated by hydrogen diffusion in the alloy and internal resistance of the battery, including ohmic internal resistance and polarization reduces with the increase of the diffusion coefficient of the hydrogen atom. The influence of milling time on the diffusion coefficient of hydrogen atoms will be discussed in the next section.

The discharge capacity of the as-cast and milled  $Y_0$  and  $Y_3$  alloys as a function of milling time is described in Fig. 5, from which it is found that the variation trend of the discharge capacity of the alloys with milling time is different. For the  $Y_0$  alloy, the discharge capacity increases with milling time prolonging, while for the  $Y_3$  alloy, it has the maximum value in the same condition. The latter indicates that mechanical milling makes a beneficial and detrimental impact on the discharge capacity. Therein, the positive contribution is definitely ascribed to the formation of nanocrystalline structure due

to the fact that ultrafine grains created by mechanical milling give rise to a great number of grain boundaries in which a substantial fraction of atoms are located [18]. Also, CUI et al [19] revealed that nanocrystalline Mg<sub>2</sub>Ni alloys can electrochemically absorb and desorb a large amount of hydrogen at room temperature. The negative action caused by mechanical milling on the discharge capacity is ascribed to the following two aspects: firstly, extending milling time positively causes lattice strain, which will continually accumulate with milling process up to forming the deformation and distortion of crystal lattice, as shown in Fig. 3(f). Consequently, the number of hydrogen occupation sites is enormously reduced, hence decreasing the discharge capacity [20]. Secondly, prolonging milling time facilitates forming amorphous phase, which is disadvantageous to capacity due to the fact confirmed by ORIMO and FUJII [21] that the amorphous microstructure can accommodate smaller amounts of hydrogen than nanocrystalline one.

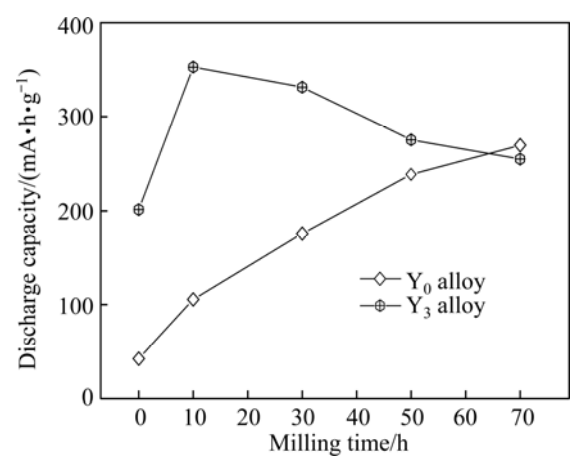


Fig. 5 Evolution of discharge capacity of  $Y_0$  and  $Y_3$  alloys with milling time

#### 3.2.2 Electrochemical cycle stability

Generally, the electrochemical cyclic stability, one of evaluation indicators whether or not an electrode material can be applied to Ni-MH batteries, is characterized by capacity retaining rate  $(S_n)$ , which is defined as  $S_n = (C_n/C_{\text{max}}) \times 100\%$ , where  $C_{\text{max}}$  is the maximum discharge capacity and  $C_n$  is the discharge capacity of the nth charge-discharge cycle at a current density of 40 mA/g. The  $S_n$  values of the as-milled  $Mg_{20-x}Y_xNi_{10}$  (x=0-4) alloys as a function of cycle number are described in Fig. 6. As can be seen, the  $S_n$ values of the alloys visibly decrease with increasing cycle number, and mechanical milling makes the degradation rate of discharge capacity of the alloys increase obviously, suggesting that mechanical milling makes a negative contribution to the cycle stability of the alloys. To directly show the effects of milling time on the cycle stability of the alloys, the relationships between the

 $S_{20}$  (n=20) value and the milling time are presented in Figs. 6(a) and (b), respectively. It is obvious that the  $S_{20}$  value clearly decreases with milling time prolonging. To be specific, increasing milling time from 0 (as-cast is defined as milling time of 0 h) to 70 h results in a decrease in the  $S_{20}$  value from 43.6% to 33.9% for the  $Y_0$  alloy and from 86.7% to 65.9% for the  $Y_3$  alloy. In addition, comparing Figs. 6(a) with (b), it is found that for all the milling time, the  $S_{20}$  value of the  $Y_3$  alloy is much larger than that of the  $Y_0$  alloy, indicating that Y substitution for Mg engenders a positive contribution to the cycle stability of the Mg<sub>2</sub>Ni alloy.

As is well known, the major reason leading to the sharp degradation of the discharge capacity of Mg<sub>2</sub>Ni alloy is ascribed to the following two aspects: on one hand, Mg(OH)<sub>2</sub> layer on the surface of the alloy electrode continuously forms and thickens with cycle number increasing, which hinders hydrogen atoms from diffusing in or out in alkaline solution [22]; on the other hand, hydrogen storage material suffers from an inevitable volume expansion and contraction during the

charge/discharge process, resulting in the cracking and pulverizing of the alloy, which in turn, makes the surface of the material apt to be oxidized. To reveal the failure mechanism of the experimental alloy, the morphologies of the alloy particles before and after electrochemical cycling are examined by SEM, as demonstrated in Fig. 7. It is found that a rough and flocculent layer covers the full surface of the alloy particles after electrochemical cycling, which is determined to be Mg(OH)2 by XRD detection, as presented in Fig. 7(c). Thereby, it would be reasonable to believe that the formation of the rough and flocculent layer is an important reason for the capacity deterioration of the alloys. As to the negative impact caused by mechanical milling, it is convinced to be ascribed to forming the nanocrystalline structure and producing the lattice strain resulted from milling due to fact that the corrosion resistance of the nanostructured alloy is quite poor [23]. Furthermore, the positive contribution of Y substitution for Mg to the cycle stability is most likely ascribed to the following several aspects. Firstly, the rare earth elements (La, Nd,

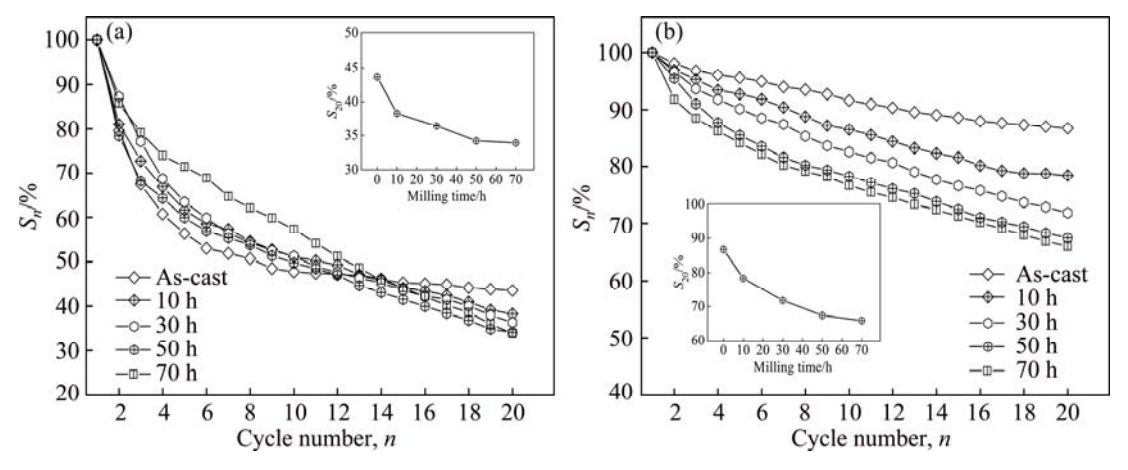


Fig. 6 Evolution of capacity retaining rates  $(S_n)$  of as-cast and milled  $Mg_{20-x}Y_xNi_{10}$  alloys with cycle number: (a)  $Y_0$  alloy; (b)  $Y_3$  alloy

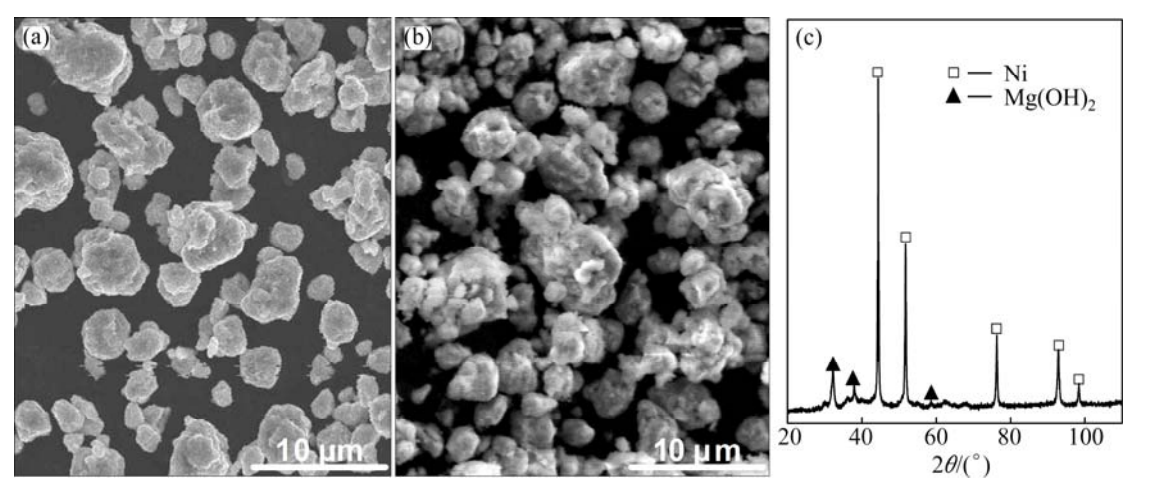


Fig. 7 SEM morphologies and typical XRD pattern of as-milled (30 h) Y<sub>3</sub> alloys before and after electrochemical cycle: (a) Before cycling; (b) After cycling; (c) XRD pattern after cycling

Sm and Y) can be dissolved in the Mg<sub>2</sub>Ni alloy, just as the EDS pattern shown in Fig. 1(a), which can enlarge the cell volume of the Mg<sub>2</sub>Ni alloy easily [24], then decreasing the ratios of expansion/contraction in the process of hydrogen absorption/desorption, and thus enhancing the anti-pulverization capability. Secondly, the partial substitution of Y for Mg can improve the resistance of the alloy against corrosion in alkaline solution and increase the cycle life of the alloy [25]. which is considered to be associated with the formation of a dense and protective yttrium oxide on the alloy surface that suppresses further oxidation of Mg and induces a Ni-enriched layer on the alloy surface [2]. In addition, the change of the major phase of the alloy caused by Y substitution for Mg is the other important reason due to the confirmed fact that LaMgNi4 phase possesses much higher cycle stability than Mg<sub>2</sub>Ni.

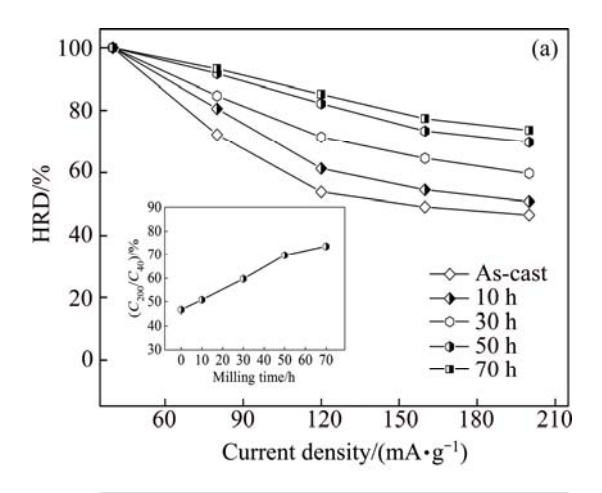
#### 3.2.3 Electrochemical kinetics

Generally, the electrochemical kinetics of an alloy electrode is symbolized by its high rate discharge (HRD), defined as HRD= $(C_i/C_{40})\times 100\%$ , where  $C_i$  and  $C_{40}$  are the maximum discharge capacities of the alloy electrode charged-discharged at current densities of i and 40 mA/g, respectively. The HRD of the as-cast and milled Mg<sub>20-x</sub>Y<sub>x</sub>Ni<sub>10</sub> alloys as a function of current density is described in Fig. 8. It is evident that the HRDs of the electrode alloys decline in different degrees with the current density increasing. Maintaining a high discharge capacity even during the process of charge-discharge cycles with a large current density is necessary for the practical application of an alloy electrode in Ni-MH battery, especially power battery. It is noted that milling time has an obvious effect on the HRD of the alloys. On the basis of the data in Fig. 8 at a current density of 200 mA/g, the relationships between the HRD of the alloys and the milling time can be established, as presented in Figs. 8(a) and (b), respectively. Apparently, the variation tendencies of the HRD of the Y<sub>0</sub> and Y<sub>3</sub> alloys with milling time are completely opposite. To be specific, prolonging milling time from 0 to 70 h brings on an increase in the HRD from 46.6% to 73.6% for the Y<sub>0</sub> alloy but a decrease from 78.7% to 61.4% for the Y<sub>3</sub>

The electrochemical hydriding/dehydriding reaction taking place at the hydrogen storage electrode in an alkaline solution during charging and discharging can be described as follows:

$$M + \frac{x}{2}H_2O + \frac{x}{2}e \leftrightarrow MH_x + \frac{x}{2}OH^-$$
 (1)

where M is the hydrogen storage alloy. Equation (1) indicates that when the alloy electrode is charged in KOH solution, hydrogen atoms adhering at the interface of alloy/electrolyte diffuse into bulk alloy and then store



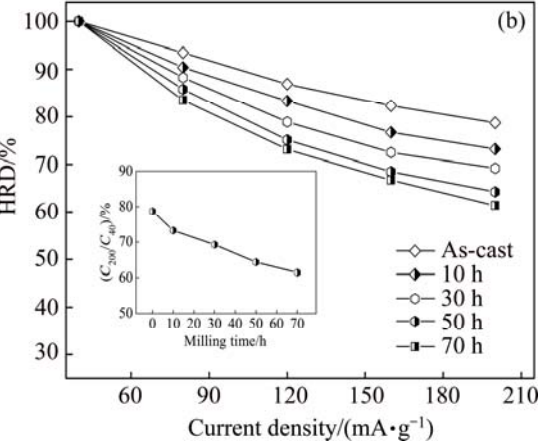


**Fig. 8** Evolution of HRDs of as-cast and milled  $Mg_{20-x}Y_xNi_{10}$  alloys with current density: (a)  $Y_0$  alloy; (b)  $Y_3$  alloy

themselves in the metallic lattice in the form of hydride. In the process of discharging, the hydrogen atoms stored in the bulk alloy diffuse toward the alloy electrode surface where it is oxidized. This indicates that electrochemical hydrogen storage kinetics of the alloy electrode is dependent on the hydrogen diffusion capability in the alloy bulk and the charge-transfer rate on the surface of an alloy electrode, as considered by CUI and LUO [26]. Hence, to reveal the mechanism of the electrochemical kinetics of the alloy, it is very necessary to investigate the effects of milling time on the diffusion ability of hydrogen atoms charge-transfer rate.

The hydrogen diffusion coefficient, which is used to symbolize hydrogen diffusion ability, could be calculated easily through the slope of the linear region of the semilogarithmic curves of anodic current density versus working duration of an alloy electrode according to [27]

$$\lg J = \lg \left( \pm \frac{6FD}{da^2} (C_0 - C_s) \right) - \frac{\pi^2}{2.303} \frac{D}{a^2} t$$
 (2)

$$D = -\frac{2.303a^2}{\pi^2} \frac{d \lg J}{dt}$$
 (3)

where J is the diffusion current density, D is the

hydrogen diffusion coefficient,  $C_0$  is the initial hydrogen concentration in the bulk of the alloy,  $C_s$  is the hydrogen concentration on the surface of the alloy particles, a is the alloy particle radius, d is the density of the hydrogen storage alloy, t is the discharge time. Figure 9 shows the semilogarithmic curves of anodic current versus working duration of the as-cast and milled Y<sub>0</sub> and Y<sub>3</sub> alloys. The D values of the alloys derived by Eq. (3) as a function of milling time are also provided in Fig. 9. It can be seen that the variation trend of the D values of the Y<sub>0</sub> and Y<sub>3</sub> alloys with milling time is opposite, which is very similar to that of the HRDs of the alloys with milling time. This shows that the diffusion ability of hydrogen atoms is a very important factor affecting the electrochemical kinetics of the alloy. FENG and NORTHWOOD [28] considered that the diffusion coefficient of hydrogen atoms in the metallic lattices is strongly associated with the strength metal-hydrogen interaction and the structure of the alloy. For the Y<sub>0</sub> alloy, the improved hydrogen diffusion ability by milling is ascribed to the refinement of the grains. The crystalline alloy, when mechanically milled, becomes at least partially disordered, yielding the

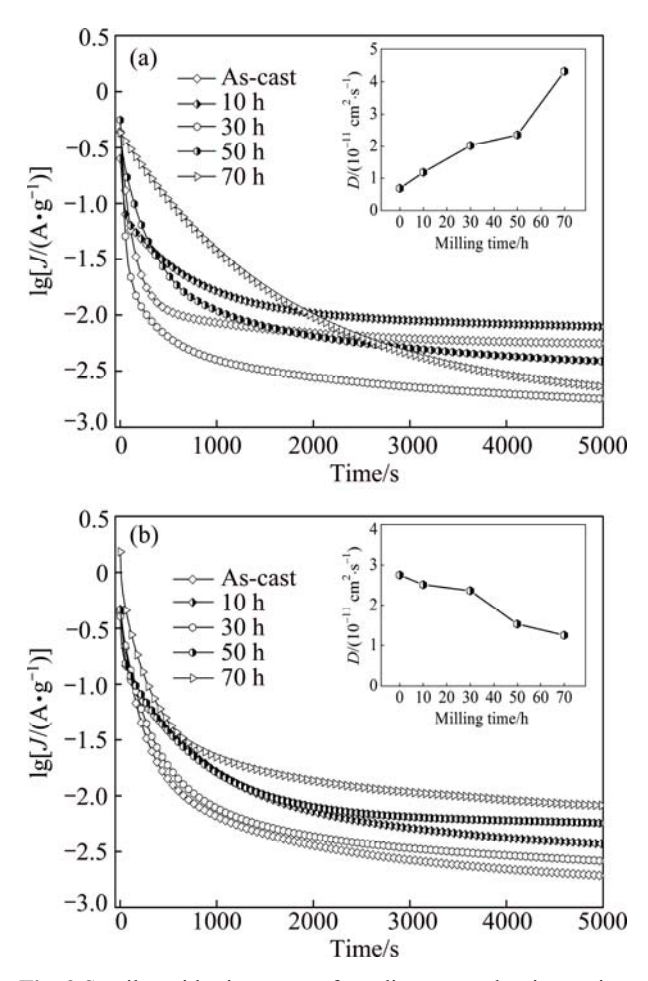


**Fig. 9** Semilogarithmic curves of anodic current density vs time responses of as-cast and milled  $Mg_{20-x}Y_xNi_{10}$  alloys: (a)  $Y_0$  alloy; (b)  $Y_3$  alloy

ultrafine grains. By refining the microstructure, a lot of new crystallites and grain boundaries are created which can act as fast diffusion paths for hydrogen transport. For the  $Y_3$  alloy, the impaired diffusion ability by milling is attributed to the facilitated glass forming by substituting Mg with Y due to the fact that the diffusion ability of hydrogen atoms in an amorphous phase is much lower than that in a nanocrystalline phase [29]. The amount of the amorphous phase grows with increasing milling time. Hence, it is easy to understand that the diffusion coefficient of the  $Y_3$  alloy declines with milling time prolonging.

Limiting current density  $(J_L)$ , another important electrochemical kinetic parameter associated with diffusion rate of hydrogen, can be derived by measuring the Tafel polarization curve, as depicted in Fig. 10. Evidently, in all cases, each anodic polarization curve has a clear inflection point, namely the existence of a critical value, which is termed as  $J_L$ . It is viewed as the result of an oxidation reaction taking place on the surface of the alloy electrode, and the oxidation layer hinders hydrogen atoms from further penetrating [30]. Thus, the limiting current density can be regarded as a critical current density for passivating. According to the experiment results provided in Fig. 10, the relationships between the  $J_L$  values of the  $Y_0$  and  $Y_3$  alloys and the milling time can be established, just as exhibited in Figs. 10(a) and (b), respectively. It is evident that the  $J_L$ value of the Y<sub>0</sub> alloy augments with increasing milling time, but it clearly declines in the same condition for the Y<sub>3</sub> alloy.

As to charge-transfer ability of the surface of an alloy electrode, it can be qualitatively evaluated through measuring EIS by means of the Kuriyama's model [31]. The EIS curves of the as-cast and milled  $Mg_{20-x}Y_xNi_{10}$ alloys are presented in Fig. 11. It is found that each EIS has two distorted capacitive loops in the high and middle frequency regions separately as well as a line in the low frequency region, which very well represents the electrochemical process of the alloy electrode. Among them, the smaller semicircle in the high frequency region reflects the contact resistance between the alloy powder and the conductive material, and the larger one in the frequency region corresponds middle charge-transfer resistance on the alloy surface while the straight line in the low frequency region represents the atomic hydrogen diffusion in the alloy. In view of this, the charge-transfer ability can be evaluated easily, namely the larger the radius of the semicircle in the middle frequency region is, the higher the charge-transfer resistance of the alloy electrode will be. It can be seen from Fig. 11 that the radii of the large semicircles in the middle frequency region for the Y<sub>0</sub> alloy significantly

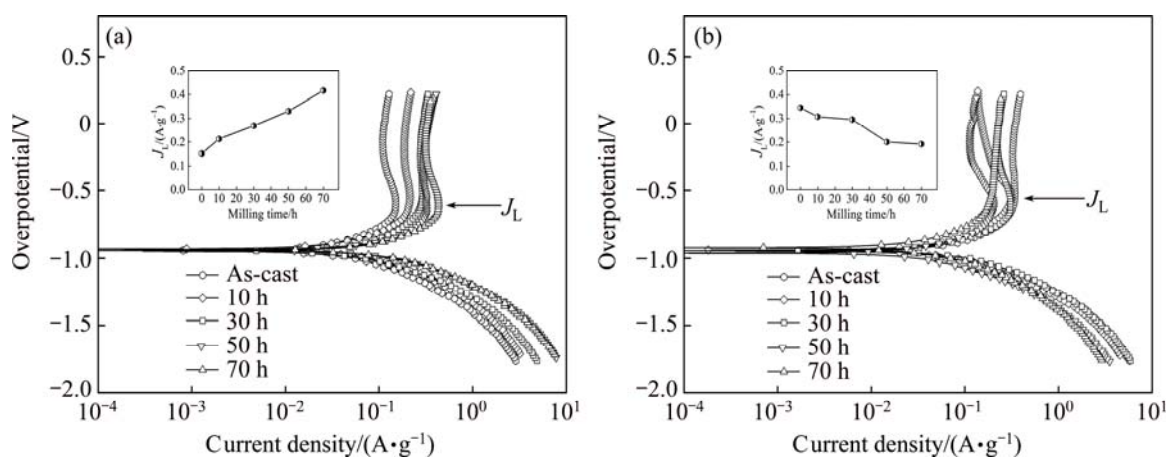


Fig. 10 Tafel polarization curves of as-cast and milled  $Mg_{20-x}Y_xNi_{10}$  alloys: (a)  $Y_0$  alloy; (b)  $Y_3$  alloy

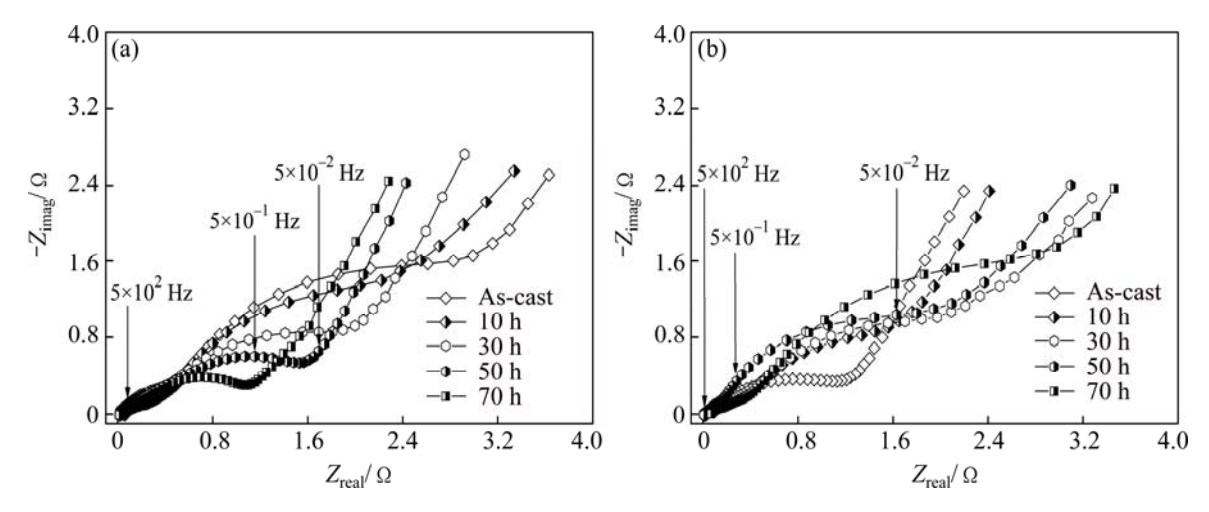


Fig. 11 EIS of as-cast and milled  $Mg_{20-x}Y_xNi_{10}$  alloys: (a)  $Y_0$  alloy; (b)  $Y_3$  alloy

shrink with milling time prolonging, while for the Y<sub>3</sub> alloy, the result is completely opposite. As considered by KLEPERIS et al [32], the charge-transfer rate depends on both crystallographic and electronic structures jointly. Thereby, the positive impact of mechanical milling on the charger transfer ability of the Y<sub>0</sub> alloy is most likely associated with following factors: firstly, the mechanical milling fundamentally modifies the surface state of the alloy powder, and especially a great number of crystal defects are created, which are very beneficial to accelerating the charge transfer; secondly, mechanical milling makes the sizes of the alloy powders dramatically decrease, increasing the interface area of the alloy particle surface and the electrolyte. The adverse effect incurred by milling on the charge transfer of the Y<sub>3</sub> alloy is most probably ascribed to the facilitated amorphous phase by increasing Y content since an amorphous phase can strongly prohibit the pulverization of the alloy during charge-discharge cycle [33], reducing available new surface of the alloy electrode and lessening charge transfer rate at the alloy-electrolyte interface.

## **4 Conclusions**

- 1) Nanocrystalline and amorphous  $Mg_2Ni$ -type  $Mg_{20-x}Y_xNi_{10}$  (x=0-4) alloys were successfully prepared by mechanical milling. The variation of milling time exerts an obvious effect on the microstructures of the alloys. Especially, the grain sizes of the alloys were dramatically refined with milling time prolonging. Furthermore, with milling time prolonging, some crystal defects were created, and deformation and distortion of the crystal lattice were clearly observed.
- 2) The effect of milling time on the electrochemical performances is dependent on the composition of the alloy. The discharge capacity of the Y-free alloy always increases with milling time extending, but that of the Y-substituted alloy has a maximum value with Y content varying. The electrochemical cycle stability of the alloys more or less declines with increasing milling time, for which the impaired corrosion resistance by forming nanocrystalline structure is basically responsible.
  - 3) Furthermore, the effect of milling time on the

electrochemical kinetics of the alloys is closely associated with Y content in the alloy. For the  $Y_0$  alloy, the electrochemical kinetics, including HRD, diffusion coefficient and charge transfer rate, clearly increase with milling time prolonging. But for the  $Y_3$  alloy, the result is completely opposite.

#### References

- KIM J S, LEE C R, CHOI J W, KANG S G. Effects of F-treatment on degradation of Mg<sub>2</sub>Ni electrode fabricated by mechanical alloying [J]. Journal of Power Sources, 2002, 104(2): 201–207.
- [2] RUGGERI S, ROUE L, HUOT J, SCHULZ R, AYMARD U, TARASCON J M. Properties of mechanically alloyed Mg-Ni-Ti ternary hydrogen storage alloys for Ni-MH batteries [J]. Journal of Power Sources, 2002, 112(2): 547-556.
- [3] JAIN I P, LAL C, JAIN A. Hydrogen storage in Mg: A most promising material [J]. International Journal of Hydrogen Energy, 2010, 35(10): 5133-5144.
- [4] JURCZYK M, SMARDZ L, OKONSKA I, JANKOWSKA E, NOWAK M, SMARDZ K. Nanoscale Mg-based materials for hydrogen storage [J]. International Journal of Hydrogen Energy, 2008, 33(1): 374–380.
- [5] WOO J H, LEE K S. Electrode characteristics of nanostructured Mg<sub>2</sub>Ni-type alloys prepared by mechanical alloying [J]. Journal of the Electrochemical Society, 1999, 146(3): 819–823.
- [6] TAKAHASHI Y, YUKAWA H, MORINAGA M. Alloying effects on the electronic structure of Mg<sub>2</sub>Ni intermetallic hydride [J]. Journal of Alloys and Compounds, 1996, 242(1–2): 98–107.
- [7] WANG Z M, ZHOU H Y, GU Z F, CHENG G, YU A B. Preparation of Mg<sub>2-x</sub>RE<sub>x</sub>Ni (RE=La, Ce, Pr, Nd, Y) alloys and their electrochemical characteristics [J]. Journal of Alloys and Compounds, 2004, 381(1–2): 234–239.
- [8] WU M S, WU H R, WANG Y Y, WAN C C. Surface treatment for hydrogen storage alloy of nickel/metal hydride battery [J]. Journal of Alloys and Compounds, 2000, 302(1-2): 248-257.
- [9] WANG Y, QIAO S Z, WANG X. Electrochemical hydrogen storage properties of ball-milled NdMg<sub>12</sub> alloy with Ni powders [J]. International Journal of Hydrogen Energy, 2008, 33(3): 1023–1027.
- [10] ZALUSKI L, ZALUSKA A, STRÖM-OLSEN J O. Nanocrystalline metal hydrides [J]. Journal of Alloys and Compounds, 1997, 253–254: 70–79.
- [11] SPASSOV T, RANGELOVA V, NEYKOV N. Nanocrystallization and hydrogen storage in rapidly solidified Mg-Ni-RE alloys [J]. Journal of Alloys and Compounds, 2002, 334(1-2): 219-223.
- [12] KALINICHENKA S, RÖNTZSCH L, RIEDL T, GEMMING T, WEIßGÄRBER T, KIEBACK B. Microstructure and hydrogen storage properties of melt-spun Mg-Cu-Ni-Y alloys [J]. International Journal of Hydrogen Energy, 2011, 36(2): 1592-1600.
- [13] ZHANG Yang-huan, SONG Chun-hong, REN Hui-ping, LI Zhi-gang, HU Feng, ZHAO Dong-liang. Enhanced hydrogen storage kinetics of nanocrystalline and amorphous Mg<sub>2</sub>Ni-type alloy by substituting Ni with Co [J]. Transactions of Nonferrous Metals Society of China, 2011, 21(9): 2002–2009.
- [14] ZHANG Yang-huan, LÜ Ke, ZHAO Dong-liang, GUO Shi-hai, QI Yan, WANG Xin-lin. Electrochemical hydrogen storage characteristics of nanocrystalline and amorphous Mg<sub>2</sub>Ni-type alloys prepared by melt-spinning [J]. Transactions of Nonferrous Metals Society of China, 2011, 21(3): 502–511.
- [15] HUANG L J, LIANG G Y, SUN Z B, WU D C. Electrode properties of melt-spun Mg-Ni-Nd amorphous alloys [J]. Journal of Power Sources, 2006, 160(1): 684-687.
- [16] LASS ERIC A. Hydrogen storage measurements in novel Mg-based nanostructured alloys produced via rapid solidification and devitrification [J]. International Journal of Hydrogen Energy, 2011,

- 36(17): 10787–10796.

  [17] LAI W H, YU C Z. Research survey of improving discharge voltage
- [17] LAI W H, YU C Z. Research survey of improving discharge voltage platform for Ni-MH battery [J]. Battery Bimonthly, 1996, 26(4): 189–191.
- [18] SPASSOV T, LYUBENOVA L, KÖSTER U, BARÓ M D. Mg-Ni-RE nanocrystalline alloys for hydrogen storage [J]. Materials Science and Engineering A, 2004, 375–377: 794–799.
- [19] CUI N, LUAN B, ZHAO H J, LIU H K, DOU S X. Effects of yttrium additions on the electrode performance of magnesium-based hydrogen storage alloys [J]. Journal of Alloys and Compounds, 1996, 233(1-2): 236-240.
- [20] ENDO D, SAKAKI K, AKIBA E. Formation of lattice strain in MmNi<sub>4,30-x</sub>Co<sub>x</sub>Al<sub>0,30</sub>Mn<sub>0,40</sub> (*x*=0, 0.75) during hydrogenation [J]. International Journal of Hydrogen Energy, 2007, 32(17): 4202–4208.
- [21] ORIMO S, FUJII H. Materials science of Mg-Ni-based new hydrides [J]. Applied Physics A, 2001, 72(2): 167–186.
- [22] ZHANG Yang-huan, LI Peng-xin, YANG Tai, ZHAI Ting-ting, YUAN Ze-ming, GUO Shi-hai. Effects of substituting La with M (M=Sm, Nd, Pr) on electrochemical hydrogen storage characteristics of A<sub>2</sub>B<sub>7</sub>-type electrode alloys [J]. Transactions of Nonferrous Metals Society of China, 2014, 24(12): 4012–4022.
- [23] SIMIČIĆ M V, ZDUJIĆ M, DIMITRIJEVIĆ R, NIKOLIĆ-BUJANOVIĆ L, POPOVIĆ N H. Hydrogen absorption and electrochemical properties of Mg<sub>2</sub>Ni-type alloys synthesized by mechanical alloying [J]. Journal of Power Sources, 2006, 158(1): 730–734.
- [24] ZHANG Yang-huan, YANG Tai, BU Wen-gang, CAI Ying, ZHANG Guo-fang, ZHAO Dong-liang. Effect of Nd content on electrochemical performances of nanocrystalline and amorphous (Mg<sub>24</sub>Ni<sub>10</sub>Cu<sub>2</sub>)<sub>100-x</sub>Nd<sub>x</sub> (x=0-20) alloys prepared by melt spinning [J]. Transactions of Nonferrous Metals Society of China, 2013, 23(12): 3668–3676.
- [25] LENAIN C, AYMARD L, DUPONT L, TARASCON J M. A new  $Mg_{0.9}Y_{0.1}Ni$  hydride forming composition obtained by mechanical grinding [J]. Journal of Alloys and Compounds, 1999, 292(1–2): 84–89
- [26] CUI N, LUO J L. Electrochemical study of hydrogen diffusion behavior in Mg<sub>2</sub>Ni-type hydrogen storage alloy electrodes [J]. International Journal of Hydrogen Energy, 1999, 24(1): 37–42.
- [27] ZHENG G, POPOV B N, WHITE R E. Electrochemical determination of the diffusion coefficient of hydrogen through an LaNi<sub>4.25</sub>Al<sub>0.75</sub> electrode in alkaline aqueous solution [J]. Journal of the Electrochemical Society, 1995, 142(8): 2695–2698.
- [28] FENG F, NORTHWOOD D O. Hydrogen diffusion in the anode of Ni/MH secondary batteries [J]. Journal of Power Sources, 2004, 136(2): 346–350.
- [29] XIE D H, LI P, ZENG C X, SUN J W, QU X H. Effect of substitution of Nd for Mg on the hydrogen storage properties of Mg<sub>2</sub>Ni alloy [J]. Journal of Alloys and Compounds, 2009, 478(1–2): 96–102.
- [30] ZHAO X Y, DING Y, MA L Q, WANG L Y, YANG M, SHEN X D. Electrochemical properties of MmNi<sub>3.8</sub>Co<sub>0.75</sub>Mn<sub>0.4</sub>Al<sub>0.2</sub> hydrogen storage alloy modified with nanocrystalline nickel [J]. International Journal of Hydrogen Energy, 2008, 33(22): 6727–6733.
- [31] KURIYAMA N, SAKAI T, MIYAMURA H, UEHARA I, ISHIKAWA H, IWASAKI T. Electrochemical impedance and deterioration behavior of metal hydride electrodes [J]. Journal of Alloys and Compounds, 1993, 202(1-2): 183-197.
- [32] KLEPERIS J, WÓJCIK G, CZERWINSKI A, SKOWRONSKI J, KOPCZYK M, BELTOWSKA-BRZEZINSKA M. Electrochemical behavior of metal hydrides [J]. Journal of Solid State Electrochemistry, 2001, 5(4): 229–249.
- [33] ZHANG Yang-huan, XU Sheng, ZHAI Ting-ting, YANG Tai, YUAN Ze-ming, ZHAO Dong-ling. Hydrogen storage kinetics of nanocrystalline and amorphous Cu-Nd-added Mg<sub>2</sub>Ni-type alloys [J]. Transactions of Nonferrous Metals Society of China, 2014, 24(11): 3524–3533.

# Ni-MH 电池用 Mg-Y-Ni 纳米晶和 非晶合金的电化学性能

张羊换1,2, 韩忠刚1,2, 袁泽明2, 杨泰2, 祁焱2, 赵栋梁2

- 1. 内蒙古科技大学 内蒙古自治区白云鄂博矿多金属资源综合利用重点实验室,包头 014010;
  - 2. 钢铁研究总院 功能材料研究所, 北京 100081

摘 要:采用真空感应熔炼在高纯氦气气氛保护下制备  $Mg_2Ni$ 型  $Mg_{20-x}Y_xNi_{10}$  (x=0,1,2,3,4) 铸态电极合金,然后将铸态合金置于行星式球磨机中进行机械球磨得到球磨合金。SEM、XRD 以及 TEM 测试结果表明,通过球磨可以得到纳米晶和非晶结构,非晶相含量随着球磨时间的延长而增加。电化学测试表明, $Y_0$ 合金的放电容量随着球磨时间的延长而增大,而 Y 替代合金的放电容量随球磨时间的延长出现最大值。循环稳定性随着球磨时间的延长均有所降低,表明球磨对循环稳定性不利。球磨时间对电化学动力学的影响与 Y 含量有关。当 x=0 时,合金电极的高倍率放电性能、氢扩散系数、极限电流密度以及电荷转移率都随着球磨时间的延长而增大,而 x=3 时结果却相反。

关键词: 贮氢; Mg2Ni 型合金; 机械球磨; 元素替代; 电化学性能

(Edited by Xiang-qun LI)